International Journal of Modern Physics B
Vol. 20, Nos. 11, 12 & 13 (2006) 1648–1660

World Scientific
www.worldscientific.com

TRANSLATIONAL ENTANGLEMENT BY COLLISIONS AND HALF-COLLISIONS

LIOR FISCH
Department of Chemical Physics, The Weizmann Institute of Science
Rehovot 76100, Israel
lior.fisch@weizmann.ac.il

ASSAF TAL
Department of Chemical Physics, The Weizmann Institute of Science
Rehovot 76100, Israel
assaf.tal@weizmann.ac.il

GERSHON KURIZKI
Department of Chemical Physics, The Weizmann Institute of Science
Rehovot 76100, Israel
gershon.kurizki@weizmann.ac.il

Received 12 September 2005
Revised 29 October 2005

Here we aim at setting the principles of and quantifying translational entanglement by collisions and half-collisions. In collisions, the resonance width s and the initial phase-space distributions are shown to determine the degree of post-collisional momentum entanglement. Half-collisions (dissociation) are shown to yield different types of approximate EPR states. We analyse a feasible realization of translational EPR entanglement and teleportation via cold-molecule Raman dissociation and subsequent collisions, resolving both practical and conceptual difficulties it has faced so far.

Keywords: Entanglement; continuous variables; teleportation; EPR correlations.

1. Introduction

Despite the fact that entanglement and EPR-like correlations have become key notions in contemporary physics, the original EPR scenario,[1] namely, two-particle entanglement involving continuous variables,[2] has been studied much later than the discrete-variable spin-1/2 entanglemnt.[2–12] The first concrete proposal for measuring position-momentum entanglement of *massive unbound* particles was made by Opatrný and Kurizki[7] based on molecular-dimer dissociation. They also suggested that a subsequent collision of one of the EPR-entangled dissociation fragments with a wavepacket, followed by Bell-like measurements of their *joint* variables, can be used to teleport the wavepacket.

Here we set a broader aim: understanding and quantifying the entanglement of the translational degrees of freedom of the particles, by studying a ubiquitous class of processes, namely, binary collisions of *unbound particles* based on the recent analysis of Tal and Kurizki[8] and comparing them to half-collisions (bound-state dissociation). We shall address both practical and conceptual difficulties these processes may face. The considerations outlined here are common to molecular dissociation,[7–9] dipole-dipole correlations in optical lattices,[10,11] photoionization[12] and cold-atom collisions.[13,14]

2. EPR States and Measures

The two possible EPR states of particles 1, 2 with *ideal* coordinate and momentum entanglement will be denoted by $|EPR_{\mp}\rangle$. They satisfy

$$\begin{aligned}\langle x_1, x_2|EPR_{\mp}\rangle &= \delta(x_1 \mp x_2)\\ \langle p_1, p_2|EPR_{\mp}\rangle &= \delta(p_1 \pm p_2)\end{aligned} \tag{1}$$

where $x_{1(2)}$ and $p_{1(2)}$ are the respective coordinates and momenta. Both these states are unrealistic, in that they are unnormalizable and have infinite energy. They may be seen as limits of the "physical" state

$$\langle x_1, x_2|\Psi\rangle = Ne^{-(\frac{x_{cm}}{2\Delta x_{cm}})^2}e^{-(\frac{x_{rel}}{2\Delta x_{rel}})^2} \tag{2}$$

where N is the normalization, $x_{rel} \equiv x_1 - x_2$ and $x_{cm} \equiv \frac{x_1+x_2}{2}$ are the relative and center-of-mass coordinates. The limit $\Delta x_{rel} \to 0, \Delta x_{cm} \to \infty$ yields the EPR$_-$ state and the limit $\Delta x_{rel} \to \infty, \Delta x_{cm} \to 0$ yields its EPR$_+$ counterpart.

The degree to which state (2) approximates the ideal states (1) can be quantified by several criteria. Opatrný and Kurizki[7] adopted the "squeezing" parameter s, defined as

$$s(t) = \frac{\hbar}{2\Delta x_1^{(c)}(t)\Delta p_1^{(c)}}. \tag{3}$$

$\Delta x_1^{(c)}$ is the variance of the *conditional* distribution

$$P(x_1|x_2 = a) = \frac{|\Psi(x_1, x_2 = a)|^2}{P(x_2 = a)}, \tag{4}$$

and $P(x_2 = a) = \int dx_1 |\Psi(x_1, x_2 = a)|^2$. Similarly, $\Delta p_1^{(c)}$ is the conditional momentum uncertainty.

Alternatively, the *largest* of $\Delta x_{rel}/\Delta x_{cm}$, or its inverse (likewise for $\Delta p_{rel}/\Delta p_{cm}$) may define $s(t)$ for the Gaussian wavepackets [Eq. (2)]. In the EPR-$_{\mp}$ limit, e.g., $s(t) = \Delta x_{rel}(t)/\Delta x_{cm}(t)$. When approaching the EPR$_+$ limit, we find $\Delta x_1^{(c)} = \min(2\Delta x_{cm}, \Delta x_{rel})$, while near the EPR$_-$ limit, $\Delta p_1^{(c)} = \min(2\Delta p_{cm}, \Delta p_{rel})$. Thus, the parameter s, which is the inverse of what may be termed the 'Einstein uncertainty', is an appropriate measure of the EPR correlation for both EPR states, occurring when $s > 1$. As $|\Psi\rangle$ in Eq. (2) *evolves*

freely, the c.m. and relative uncertainties in the r_j $(j = 1, 2)$ coordinates grow as $\Delta r_j(t)^2 = \Delta r_j(0)^2 + \Delta p_j^2 t^2/m^2$, and thus the value of s becomes *smaller* with time.

One may also measure entanglement by the Von-Neumann (VN) entropy, which, for the *discretized* eigenvalues λ_n of the single-particle reduced density matrix, has the form

$$S \equiv -\sum_{n=0}^{\infty} \lambda_n \ln \lambda_n. \tag{5}$$

The evaluation of S for collisions of unbound particles is highly nontrivial, as shown in Sec. 3. For the gaussian state (2), S becomes[3]

$$S = \log \frac{(\Delta x_{rel} + 2\Delta x_{cm})^2}{8\Delta x_{rel}\Delta x_{cm}} + \left|\frac{\Delta x_{rel} - 2\Delta x_{cm}}{4\Delta x_{rel}\Delta x_{cm}}\right| \log \left|\frac{\Delta x_{rel} + 2\Delta x_{cm}}{\Delta x_{rel} - 2\Delta x_{cm}}\right|. \tag{6}$$

In the limit $\Delta x_{cm} \gg \Delta x_{rel}$, this reduces to $S \simeq \log \Delta x_{cm}(t)/\Delta x_{rel}(t) = \log s(t)$.

While gaussian-like wavepackets in the relative and center-of-mass variables are adequately characterized by $s(t)$, S quantifies the entanglement of an *arbitrarily-shaped* (non-gaussian) wavepacket, which is common for unbound-particle collisions (Sec. 3).

A recent experiment[6] has demonstrated that $s \sim 10$ is achievable by combining a near-field measurement of Δx_{rel} with a far-field measurement of Δp_{cm} for photon pairs generated by parametric down conversion. The more formidable challenge examined here is the preparation and measurement of EPR correlations between matter waves, formed by dissociation or a collision.

3. EPR Entanglement via Two-Particle Collisions

3.1. *General description*

Consider two particles, 1 and 2, coupled by a *finite-range* interaction. Assuming that the interaction does not affect their internal states, the initial two-particle *unbound* state, $|\Psi_i\rangle$, evolves, after the interaction (collision) has ceased, as[15]

$$|\Psi_i\rangle \to |\Psi_f\rangle = (U_1(t) \otimes U_2(t))(I_{CM} \otimes \mathsf{S})|\Psi_i\rangle, \tag{7}$$

where U_j is the free-evolution propagator of system $j = 1, 2$, I_{CM} is the identity operator of the center-of-mass (CM) motion of the two systems, and S is the scattering matrix for their relative motion. The post-collision single-particle VN entropy is then obtainable as

$$(S_1)_f = -\mathrm{tr}_1(\rho_1 \log_2 \rho_1), \tag{8}$$

$$\rho_1 = \mathrm{tr}_2\left((I_{CM} \otimes \mathsf{S})|\Psi_i\rangle\langle\Psi_i|(I_{CM} \otimes \mathsf{S})^\dagger\right), \tag{9}$$

where we have used the VN entropy's invariance under unitary transformations. The entanglement is seen to be a function solely of the scattering matrix and the initial wave function. Since the diagonalization of the continuous-variable reduced density

matrix ρ_1, as required to compute $(S_1)_f$, is generally intractable, simplifications and approximations are imperative.

We shall consider two unbound particles of equal mass, such that their relative momentum is related to their individual momenta by $\mathbf{k}_{rel} = \frac{\mathbf{k}_1 - \mathbf{k}_2}{2}$. For three dimensional (3D) collisions, we shall assume that each momentum state $|\mathbf{k}_i\rangle$ can scatter onto a discrete, orthonormal set of final states with momenta $\{\mathbf{k}_f\}_{j=1}^{M}$. The replacement of continuous variables by discrete values of $\mathbf{k}_f$ and $\mathbf{k}_i$ implies the use of momentum wavepackets centered around these values, whose widths are small enough (see below) for the S-matrix elements $\langle \mathbf{k}_f | \mathsf{S} | \mathbf{k}_i \rangle$ to be constant throughout the wavepacket.

Let us take the initial two-particle state to be an entangled superposition

$$|\Psi_i\rangle = \sum_i c_i |\mathbf{k}_i\rangle \otimes |-\mathbf{k}_i\rangle = \sum_i c_i |\mathbf{K}_{CM} = \mathbf{0}\rangle \otimes |\mathbf{k}_{rel} = \mathbf{k}_i\rangle. \tag{10}$$

Following the collision, Eq. (10) evolves, according to the superposition principle, into:

$$|\Psi_f\rangle = \sum_i \sum_{\mathbf{k}_f} c_i \langle \mathbf{k}_f | \mathsf{S} | \mathbf{k}_i \rangle |-\mathbf{k}_f\rangle \otimes |\mathbf{k}_f\rangle, \tag{11}$$

the sum running over $\mathbf{k}_{rel} = \mathbf{k}_f$. In the resulting post-collision density matrix $|\Psi_f\rangle\langle\Psi_f|$ of the system, particle 2 can be traced out to yield the single-particle (reduced) post-collision density operator $(\rho_1)_f = \sum_{\mathbf{k}_f} \left| \sum_i \langle \mathbf{k}_f | \mathsf{S} | \mathbf{k}_i \rangle \right|^2 |\mathbf{k}_f\rangle\langle\mathbf{k}_f|$.

On the other hand, the initial single-particle entropy in the state (10) is readily seen to be $(S_1)_i = -\sum_i |c_i|^2 \log_2 |c_i|^2$. Hence, to zeroth order in the momentum widths of the initial wavepackets, the change $\triangle S_1^{(0)}$ in the VN entropy of particle 1 as a result of the collision is:

$$\triangle S_1^{(0)} = -\sum_{\mathbf{k}_f} \left| \sum_i c_i \mathsf{S}_{\mathbf{k_f},\mathbf{k_i}} \right|^2 \log_2 \left(\left| \sum_i c_i \mathsf{S}_{\mathbf{k_f},\mathbf{k_i}} \right|^2 \right) + \sum_i |c_i|^2 \log_2 |c_i|^2, \tag{12}$$

where $\mathsf{S}_{\mathbf{k},\mathbf{k}'} \equiv \langle \mathbf{k} | \mathsf{S} | \mathbf{k}' \rangle$. In the case $c_1 = 1$, when Eq. (10) has the unentangled (product) form $|\mathbf{k}_i\rangle \otimes |-\mathbf{k}_i\rangle$, Eq. (12) reduces to:

$$\triangle S_1^{(0)} = -\sum_{\mathbf{k}_f} |\mathsf{S}_{\mathbf{k_f},\mathbf{k_i}}|^2 \log_2 \left(|\mathsf{S}_{\mathbf{k_f},\mathbf{k_i}}|^2 \right). \tag{13}$$

This result is in complete correspondence with the classical Boltzmann law for entropy change in collisions,[16] if we identify $|\mathsf{S}_{\mathbf{k_f},\mathbf{k_i}}|^2$ with the transition probability from an initial to a final momentum state. By contrast, the interferences of different scattering channels in Eq. (10) for two or more $c_i \neq 0$, render $\triangle S_1$ nonclassical.

3.2. *1D collisions*

To investigate this nonclassical behavior in-depth, we shall henceforth restrict ourselves to 1D collisions of two unbound particles with (equal) mass m. The effect of

the S-matrix on single-particle momentum eigenkets is then

$$\mathsf{S}|k\rangle = T(k)|k\rangle + R(k)|-k\rangle, \tag{14}$$

where $T(k)$ and $R(k)$ are, respectively, the transmission and reflection coefficients of the interaction potential $V(x_{rel})$.

The reduced single-particle post-collision density operator consists of four terms: two "cross terms", containing R^*T or RT^*, and two direct terms, containing RR^* and TT^*. Let us look at one of the cross terms explicitly (the R^*T term):

$$(\rho_1)^{R^*T} \int dk_1 dk_1' |k_1\rangle\langle k_1'| [\int dk R^*(\frac{k_1'-k}{2})\psi_1^*(k)\psi_2^*(k_1')T(\frac{k_1-k}{2})\psi_1(k_1)\psi_2(k)] \,. \tag{15}$$

Taking $|\Psi_i\rangle = |\psi_1\rangle \otimes |\psi_2\rangle$, where the initial wavepackets $|\psi_1\rangle, |\psi_2\rangle$ are *orthogonal*, we can simplify Eq. (9) as follows. Since $\psi_1(k)$ is a particle initially moving to the right, confined to $k > 0$, and $\psi_2(k)$ is its left-moving counterpart confined to $k < 0$, these have no overlap and the $\int dk$ integration yields 0. Hence we are left with only the "direct" terms:

$$\rho_1 = \rho_1^T + \rho_1^R, \tag{16}$$

$$\rho_1^T = \int dk_1 dk_1' dk |k_1\rangle\langle k_1'| \psi_1(k_1)\psi_1^*(k_1')|\psi_2(k)|^2 \times T\left(\frac{k_1-k}{2}\right) T^*\left(\frac{k_1'-k}{2}\right), \tag{17}$$

$$\rho_1^R = \int dk_1 dk_1' dk |k_1\rangle\langle k_1'| \psi_2(k_1)\psi_2^*(k_1')|\psi_1(k)|^2 \times R\left(\frac{k_1-k}{2}\right) R^*\left(\frac{k_1'-k}{2}\right). \tag{18}$$

Thus, the reduced post-collision ($1D$) density operator naturally splits into *transmitted* and *reflected* parts, which are orthogonal in the sense that $\rho_1^T \rho_1^R = 0$. As a result, the set of eigenvalues of ρ_1 is given by the union of the sets of eigenvalues of ρ_1^T and ρ_1^R.

In order to evaluate the *near-resonance* collisional entanglement, we perform a series expansion of ρ_1^T and ρ_1^R to second order in the momentum spread of the wavepackets, σ. The momentum spread $\Delta k^2 \equiv \langle k - k_0\rangle^2 \sim \sigma^2$, turning Eq. (12) and the eigenvalues corresponding to Eq. (16) into:

$$\triangle S_1^{(2)} = -\lambda_T^{(2)} \log_2 \lambda_T^{(2)} - \lambda_R^{(2)} \log_2 \lambda_R^{(2)}, \tag{19}$$

$$\lambda_T^{(2)} = |T(k_0)|^2 + \frac{\Delta k^2}{4}\frac{d^2}{dk^2}|T(k)|^2_{k=k_0}, \tag{20}$$

$$\lambda_R^{(2)} = |R(k_0)|^2 - \frac{\Delta k^2}{4}\frac{d^2}{dk^2}|T(k)|^2_{k=k_0}. \tag{21}$$

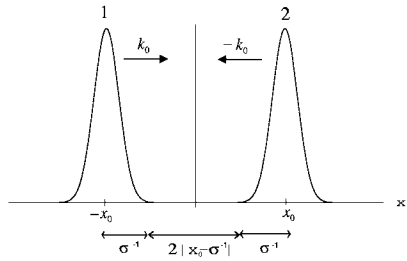

Fig. 1. Schematic illustration of a 1D collision between two wavepackets via a short-range potential, with pre-collision distance $2|x_0 - \sigma|$, momenta $\pm\hbar k_0$ and momentum spread $\hbar\sigma^{-1}$.

This analysis, verified by the numerical case study below, shows that initial narrow-width wavepackets are expected to yield double-peaks of the entanglement on both sides of a resonance, where $|T(k)|^2 = |R(k)|^2 = \frac{1}{2}$ and $T(k)$ varies strongly, with a non-zero dip at resonance. In limit $\Delta k \to 0$, the entanglement vanishes when $|T(k)| = 1$ (at resonance) or when $|R(k)| = 1$ (both wavepackets are reflected entirely).

We may estimate $\triangle S_1$ for appreciable $1D$ momentum widths, $\sigma \gg \Gamma$, i.e., when the initial wavepacket width is much larger than that of the resonance. The post-collision wavefunction can then be written as the sum of transmitted and reflected wavepackets. Each wavepacket is initially confined, in k-space, to a $1D$ region of dimensions $\Delta k \sim \sigma$. After the collision they are modulated by the transmission and reflection coefficients, the smallest scale of change for both given by Γ. Since the smallest scale of change of a function is the largest scale of change of its Fourier-transform, we can deduce that the emerging wavepackets will be confined in x-space to a box of dimensions $\Delta x_j \sim \frac{1}{\Gamma}$. Hence, we may deduce from Eq. (17)–(19) that

$$(S_j)_{max} \sim \log_2\left(\frac{\sigma}{\Gamma}\right) (j = 1, 2). \tag{22}$$

However, *the growth of* $(S_1)_{max}$ *with momentum width* σ *saturates as* σ *exceeds the distance between resonances* (in momentum space).

In order to corroborate the above analytical estimates, we perform a numerical case study, taking the interaction potential to be described by a 1D double-delta function of width a,

$$V(x_{rel}) = V[\delta(x_{rel} - a) + \delta(x_{rel} + a)]. \tag{23}$$

For small initial momentum widths, such that $\sigma \ll \Gamma$ [i.e., for the last few peaks in Fig. (2b.)), the numerical results confirm the analytical prediction (19] whereby the entropy must have a dip at resonance, $|T|^2 = 1$. On the other hand, $\triangle S_1$ is *maximal* at resonance for $\sigma \sim \Gamma$ or greater. We must control the spacing of resonances, Δk, and their widths, Γ, in order to attain

$$\Delta k \gg \sigma \gg \Gamma, \tag{24}$$

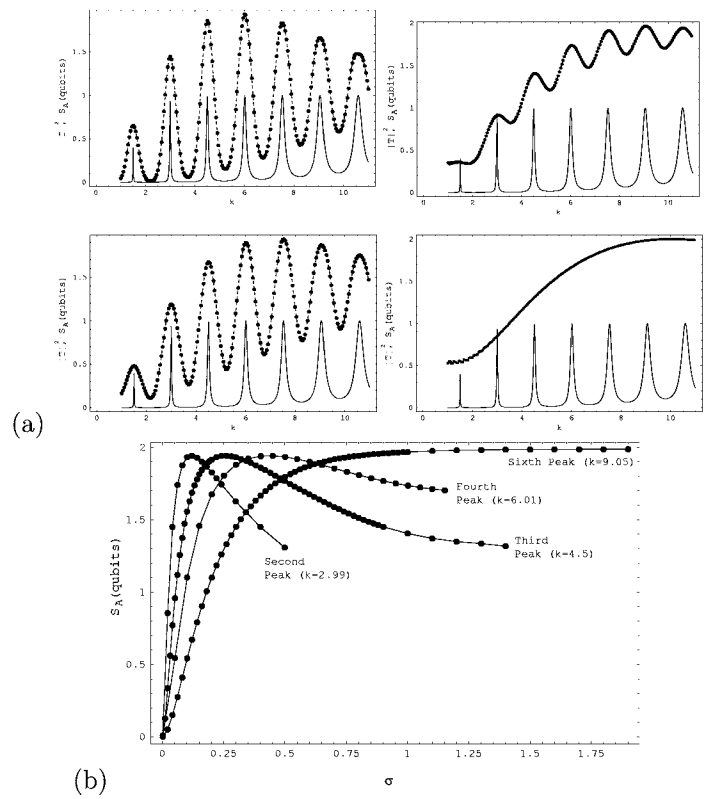

Fig. 2. (a): Simulation results for the single-particle change in VN entropy, $\triangle S_1$ in 1D collisions for the delta-function potential (23) as a function of the relative momentum. Dotted curves: left, thick curves: right. Thin curves indicate the resonances of the transmission coefficient, the peaks corresponding to $|T|^2 = 1$. Each plot corresponds to another width σ (dashed curves). (b): variation of the VN entropy as a function of the wavepacket width, σ, for three relative momenta, corresponding to peaks 2, 3 and 5 of the transmission coefficient.

which is the optimal range for large ΔS_1. Hence, practically unlimited ΔS_1, indicating an approximate translational EPR state according to Eq. (8), is anticipated for near-resonant collisions, either if the potential has a *single resonance* only (Δk very large), or if the resonance width Γ is very narrow.

The post-collisional entanglement ΔS_1 is found to be *insensitive to fluctuations* in the initial state and is thus *noise resilient.*

4. Half-Collision (Dissociation) Entanglement

The two-particle initial state, whether in a collision or a half-collision (dissociation) may be factorized as

$$\langle \vec{r}_1, \vec{r}_2 | \Psi \rangle = \langle \vec{r}_{cm} | \Phi_{cm} \rangle \langle \vec{r}_{rel} | \chi_{rel} \rangle, \tag{25}$$

where $\vec{r}_{cm} = \frac{\vec{r}_1+\vec{r}_2}{2}$ and $\vec{r}_{rel} = \vec{r}_1 - \vec{r}_2$. This separable form is retained throughout the process.

Quantifying the EPR correlations requires knowledge of the form of $|\Phi_{cm}\rangle$ and $|\chi_{rel}\rangle$, in particular their position and momentum uncertainties along a chosen axis Δx and Δp_x, at asymptotically large distances r_{rel} or times t. In what follows we shall consider the resulting x and p_x dispersion for the advantageous process of molecular Raman dissociation. Raman dissociation uses two c.w. laser beams to force a molecular transition from a bound state to the continuum, via an intermediate bound state on an excited electronic surface,[9] see Fig. 3.

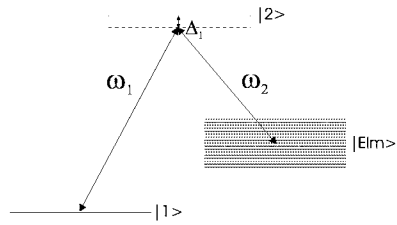

Fig. 3. 3-level model for Raman dissociation.

One then obtains the spatial form

$$\chi_{rel}(\vec{r}_{rel},t) = \sum_{l=0,2} \sqrt{\frac{2l+1}{4\pi}} P_l(\cos\theta) \quad \frac{\hbar\Omega_1\Omega^*_{2,E,l} e^{i(k_* r_{rel} - \frac{\pi l}{2} + \delta_l(E) - E_* t/\hbar)}}{2ik_* r_{rel}\Omega_{eff}}$$
$$\times\ \theta(vt - r_{rel}) \sin(\frac{\Omega_{eff}}{2}(t - \frac{r_{rel}}{v}))e^{-\frac{\Gamma}{2}(t-\frac{r_{rel}}{v})}. \tag{26}$$

This is a 1st order expansion in the continuum-level detuning. It describes a wavefunction expanding in the direction of growing r, with a sharp edge at $r_{rel} = vt$ and an exponentially falling tail at $r_{rel} < vt$. The radial width of the wavepacket is seen to be v/Γ. Equation (26) exhibits no time-dependent broadening of the wavepacket, which may therefore be treated as its *initial* post-dissociative wavepacket.

The 2nd order expansion yields a much more complicated time-dependent form, displaying dispersion of the wavepacket. An analysis of the typical time- and length-scales[12] shows that

$$t^{(spr)}_{rel} = \mu v^2/\Gamma^2\hbar \tag{27}$$

is the spreading time of the relative-motion wavepacket, which is centered at $r_{rel} \approx vt$. Thus $t/t^{(spr)}_{rel} \approx \frac{\hbar r_{rel}\Gamma^2}{v^3\mu}$ serves as a dimensionless time parameter.

In the large-spreading regime, χ_{rel} assumes a Lorentzian shape. The broadening of the wavepacket as a function of t is summarized as follows:

$$\Delta r_{rel}(t) = \begin{cases} \Delta r_{rel}^{(0)} = \frac{v_{rel}}{\Gamma}, & t \ll t_{rel}^{(spr)}, \\ v_{rel}^{(spr)} t = \frac{\hbar t}{\mu \Delta r_{rel}^{(0)}} = \frac{\hbar \Gamma}{\mu v_{rel}} t, & t \gg t_{rel}^{(spr)}. \end{cases} \tag{28}$$

The large-spreading result means that $\Delta p_{rel} = \frac{\hbar\Gamma}{v} = \Delta E_{rel} \frac{dp}{dE}$. Since the initial width of the wavepacket is $\frac{v}{\Gamma} = \hbar/\Delta p_{rel}$, the asymptotic wavefunction is found to be at its minimum uncertainty state (MUS) approximately at $t = 0$.

The pulse parameters must be taken with a view to minimizing ΔE_{rel}, the energy variance of the relative-motion wavefunction, so as to minimize $\Delta p_{rel} = \Delta E_{rel}\sqrt{\mu/2E_{rel}}$, where $\mu = m/2$ is the reduced mass of the 2 atoms: ΔE_{rel} scales with Γ, Ω_1 and the inverse of the time scale. However, ΔE_{rel} has a lower bound, since the smaller it is, the longer the time the particle stays in the excited state, and thus the larger the probability of radiative decay (spontaneous emission). Using Raman dissociation with highly monochromatic laser beams, one obtains an $|EPR_+\rangle$ - like state, characterized by $s = \Delta x_{rel}/\Delta x_{cm} \gg 1$, along with small radiative decay.

5. Post-Dissociative Dynamics

The asymptotic $|\chi_{rel}\rangle$ with low initial l, exhibits that mean relative energy $\langle E_{rel}\rangle$ and phase-shifts have little dependence on angular momentum. Due to this radial/angular *factorization*,

$$\begin{aligned} \Delta x_{rel} = \sqrt{\langle x_{rel}^2\rangle - \langle x_{rel}\rangle^2} &= \sqrt{\langle r_{rel}^2\rangle\langle\cos^2\theta\rangle - \langle r_{rel}\rangle^2\langle\cos\theta\rangle^2} \\ &> \langle r_{rel}\rangle \Delta(\cos\theta) \end{aligned} \tag{29}$$

where θ is the angle between $\vec{r}$ and the x axis.

As the angular distribution becomes more sharply peaked around $\theta = 0$, we are nearing the optimal situation, where $\Delta x_{rel} \approx \Delta r_{rel}, \Delta(p_{rel})_x \approx \Delta p_{rel}$. This is achievable by confining the atoms to a cylindrical waveguide[19] of length $2L$ and radius $R = L\tan\alpha$, lying along the x direction. The slits will only negligibly affect Φ_{cm} and its entanglement with χ_{rel} *on the x axis*, as $\Delta p_{x_{cm}} \ll \langle p_{rel}\rangle$, provided $\alpha \ll 1$. On the other hand, they will affect the shape of χ_{rel}. If the 'cylinder' is long enough, $\langle k_{rel}\rangle L \gg 1$, the effect on $\langle \vec{r}_{rel}|\psi_{rel}\rangle$ and $\langle \vec{p}_{rel}|\psi_{rel}\rangle$ can be approximated by truncating the angular distribution at $\theta = \alpha$, where

$$\alpha^2 = 4\frac{\Delta p_{rel}}{\langle p_{rel}\rangle} = \frac{2\Delta E_{rel}}{E_{rel}} \tag{30}$$

is required in order to obtain the optimal ratios $\Delta p_x = 2\Delta p_{rel}$ and $\Delta x = 2\Delta r_{rel}$. Atom pairs which have passed through the slits are correlated along the x direction, and our 1D analysis may now be applied to their dynamics.

The center of mass distribution of the molecule prior to dissociation is characterized by transverse temperature T_{cm}. The post-dissociative momentum distribution $\tilde{\phi}_{cm}(p_{cm})$ is therefore a Gaussian, $\exp[-p_x^2/2\Delta p_x^2]$, where $\Delta p_x \simeq \sqrt{2Mk_BT_{cm}}$.

Due to the dispersion (broadening) discussed above, the position and momentum correlations weaken after dissociation, and one must try to restore the initial degree of entanglement by focusing of the 2-particle wavefunction.

When the particles are well-separated and localized near $x = \pm x_0/2$, in a double-trap, with double-parabolic potential

$$V(x) = \frac{1}{2}m\omega^2(|x| - \frac{x_0}{2})^2, \tag{31}$$

the two-particle Hamiltonian has a term

$$\begin{aligned} V_{12}(x_1, x_2) &= \frac{1}{2}m\omega^2(|x_1| - \frac{x_0}{2})^2 + (|x_2| - \frac{x_0}{2})^2 \\ &= \frac{1}{2}M\omega^2 x_{c.m.}^2 + \frac{1}{2}\mu\omega^2(x_{rel} - x_0)^2 \end{aligned} \tag{32}$$

where $M = 2m$ is the total mass and $\mu = m/2$ is the reduced mass. An initially separated wavefunction of the form (2) will retain its shape while subjected to this potential.

When using a potential as in Eq. (31), we move the potentials, so that $x_0 = v_{rel}t$, where $v_{rel} = \langle p_{rel}\rangle/\mu$. This keeps the particles near the centre of the wells and avoids changing their average velocity. Both $|\Phi_{cm}\rangle$ and $|\chi_{rel}\rangle$ behave as a single particle state in a parabolic potential, and may be individually focused.

The analysis shows that the lost degree of 'squeezing' cannot be increased, but it can be preserved, by keeping the particles in the moving parabolic potentials, where Δx and Δp_x oscillate periodically. These must be turned on and start receding (moving apart) *immediately* after dissociation, and left on until measurement of the particles.

The shallowness of optically-induced potentials (typically $\approx 1mK$) drastically limits the momentum uncertainty of particles that can be stored, requiring

$$\Delta p_{rel} \ll \sqrt{2mV_{opt}} \tag{33}$$

where V_{opt} is the depth of the potential.

6. Measuring the EPR Correlations

Storage in a parabolic potential can also be used for measuring both momentum and position correlations. Leaving a particle in a parabolic potential for a quarter of the harmonic period has the effect of 'Fourier transforming' the wavefunction, as

$$\langle x|\chi_{rel}(t = \tau/4)\rangle = \sqrt{\frac{m\omega}{\hbar}}\langle p = m\omega x|\chi_{rel}(t = 0)\rangle. \tag{34}$$

After this quarter period, the new momentum distribution reflects the original x-distribution:

$$\begin{aligned} &\chi_{rel}(x_{rel} - \langle x_{rel}\rangle)\phi_{cm}(x_{cm}) \\ &\leftrightarrow \tilde{\chi}_{rel}(p_{rel} - \langle p_{rel}\rangle)\tilde{\phi}_{cm}(p_{cm}) \end{aligned} \tag{35}$$

and may be measured by time-of-flight measurement.

Verifying and measuring the EPR correlations may be done by position and momentum measurements of the two particles in large *ensembles* of such pairs. In half the pairs, the two momenta are measured by time-of-flight measurement. In the other half, the positions are measured, using Eq. (35) and time-of-flight measurement. One expects to find $\Delta x_{\mp} = \Delta(x_1 \mp x_2)$ and $\Delta p_{\pm} = \Delta(p_1 \pm p_2)$ to satisfy:

$$\Delta x_{\mp} \Delta p_{\pm} \ll \hbar/2 \tag{36}$$

in the approximate $\mathrm{EPR}_{\mp}$ state, respectively.

7. Teleportation

Obtaining a pair of correlated EPR particles (particles 2 and 3 in Fig. 4), as discussed above, is the first stage in the protocol of quantum teleportation of continuous variables.[17,18] The second stage is the measurement of the quantities $\hat{x}_- \equiv \hat{x}_1 - \hat{x}_2$ and $\hat{p}_+ \equiv \hat{p}_1 + \hat{p}_2$ (the 'Bell operators').

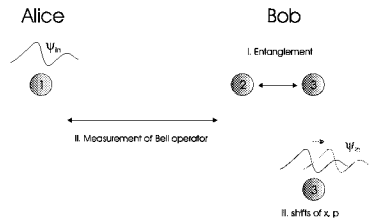

Fig. 4. Scheme of teleportation.

Opatrný and Kurizki[7] suggested performing the essentially non-local measurement of the Bell operators by a collision between the particles, followed by local measurements of the momenta. Fig. 5 schematically shows the scattering of the 'relative' coordinate, assuming a hard-sphere interaction potential, in the classical limit ($\lambda_{dB} \ll R$, where λ_{dB} is the de-Broglie wavelength of the particle and R is the radius of the hard sphere). The impact parameter x_- is related to the angle of deflection by

$$\theta = \pi - 2\sin^{-1}(x_-/R). \tag{37}$$

Since θ is the angle of the post-collisional $\vec{p}'_-$, and since $\vec{p}'_+ = \vec{p}_+$, measuring p'_1 and p'_2 is equivalent to measuring p'_+ and p'_-, and hence the pre-collisional p_{x+} and x_-. This completes the Bell measurement. One requires also $p_{z-} \gg p_{x-}$, so that the uncertainty in p_{x-} arising from measuring x_- does not significantly change the impact angle.

A measure of the accuracy of teleportation is the fidelity F, the overlap of the input state (the state to be teleported) with the teleported output. The maximal

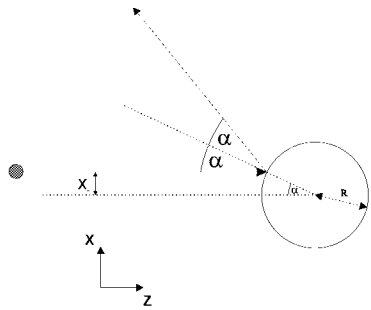

Fig. 5. KurizkiHard sphere collision.

fidelity can be shown to be $F_{max} = (1 + \Delta x_T \Delta p_T/\hbar)^{-1}$, where Δx_T and Δp_T, are the position and momentum errors incurred during the process.

The meaning of the errors Δx_T and Δp_T is that the final Wigner $x - p$ distribution $W_{out}(x_3, p_{x3})$ of the output particle is given by that of the input particle 1, $W_{in}(x_1, p_{x1})$, convoluted with a smoothing function whose width is determined by Δx_T and Δp_T:[7,18]

$$W_{out}(\alpha_3) = \int d^2\alpha \, W_{in}(\alpha) G_\sigma(\alpha_3 - \alpha) \equiv [W_{in} \circ G_\sigma](\alpha_3) \tag{38}$$

where W is presented as a function of a complex variable $\alpha \equiv x + ip$, $\circ$ denotes a convolution and $G_\sigma(\alpha)$ is a complex Gaussian of variance $\sigma = e^{-2s_T}$, $s_T \equiv \hbar/(2\Delta x_T \Delta p_T)$.

8. Conclusions

We have proposed and studied the formation of continuous-variable entanglement in controlled collisions between quasi-free particles, or quantized collective excitations, interacting as fictitious particles. Cold atoms[10,11] or slow-light polaritons,[13] free to move in 1D, but confined in the remaining 2D by an optical lattice or a waveguide, as well as small-angle collisions of fast-particles,[15] are suitable candidates.

Our comprehensive investigation of collisions has revealed the following striking conclusion: EPR entanglement is *maximized near a scattering resonance*, and grows with the phase-space volume of the initial (uncorrelated) two-system state, up to a limit determined by the spectral distance between resonances.

Specifically, the maximal amount of post-collision entanglement (VN entropy) has been shown to scale logarithmically with the position-momentum uncertainty product (phase-space volume) of the colliding wavepackets, only for *large* wavepacket widths compared to the resonances' width, but less than the distance between resonances. These results[8] show that 1D collisions yield *momentum* entangled states which, in general, *do not resemble* gaussians, but rather interfering multigaussian distributions. Nevertheless, they reveal the quantum information change via collisions of unbound particles. They also specify conditions for the

suppression of decoherence by minimization of the collision-induced entanglement. Cold-molecule Raman dissociation has been identified as a promising source of EPR gaussian-like entangled states.

Realizations involving *molecular Raman dissociation* have been argued to require the trapping of the fragments, measuring momentum-coordinate correlations (e.g., by diffraction); and finally teleportation by molecular collisions.

Acknowledgments

The support of the EC (the QUACS RTN and SCALA NOE) and ISF is acknowledged.

References

1. A. Einstein, B. Podolsky and N. Rosen, Phys. Rev. **47**, 777 (1935).
2. E. Schroedinger, *Probability relations between separated systems*, Proc. Cambridge Philos. Soc. **32**, 446-452 (1936).
3. K. W. Chan and J. H. Eberly, "Observable Phase Entanglement", quant-ph/0404093 v2 (2004); C. K. Law and J. H. Eberly, Phys. Rev. Lett. **92**, 127903 (2004).
4. J. Eisert, C. Simon and M. B. Plenio, J. Phys. A, **35**, 3911 (2002); H. Mack and M. Freyberger, Phys. Rev. A, **66**, 042113 (2002); S. Parker, S. Bose and M. B. Plenio, Phys. Rev. A, **61**, 032305 (2000); P. Horodecki and M. Lewenstein, Phys. Rev. Lett. **85**, 2657 (2000).
5. S. L. Braunstein, Phys. Rev. Lett. **80**, 4084 (1998); S. L. Braunstein and H. J. Kimble, Phys. Rev. Lett. **80**, 869 (1998).
6. J. C. Howell, R. S. Bennink, S. J. Bentley and R. W. Boyd, Phys. Rev. Lett. **92**, 210403 (2004).
7. T. Opatrný and G. Kurizki, Phys. Rev. Lett. **86**, 3180 (2001).
8. A. Tal and G. Kurizki, Phys. Rev. Lett. **94**, 160503 (2005).
9. A. Vardi and M. Shapiro, J. Chem. Phys. **104**, 5490 (1996).
10. T. Opatrny, B. Deb and G. Kurizki, Phys. Rev. Lett. **90**, 250404 (2003).
11. G. K. Brennen et al., Phys. Rev. Lett. **82**, 1060 (1999); D. Jaksch et al., *ibid* **85**, 2208 (2000); C. Moura Alves and D. Jaksch, *ibid* **93**, 110501 (2004); I. H. Deutsch *et al.*, *Quantum Computation with Neutral Atoms in an Optical Lattice*, Fortschr. Phys. **48**, 925-943 (2000).
12. Fedorov *et al*, Phys. Rev. A **69**, 052117 (2004).
13. M. Masalas and M. Fleischhauer, Phys. Rev. A **69**, 061801 (2004); I. Friedler, G. Kurizki and D. Petrosyan, Europhys Lett. **68**, 625-631 (2004).
14. I. E. Mazets, G. Kurizki, N. Katz, and N. Davidson, Phys. Rev. Lett. **94**, 190403 (2005).
15. M. L. Goldberger and K. M. Watson, *Collision Theory* (Wiley, New York, 1964).
16. L. D. Landau and E. M. Lifshitz, *Statistical Physics* (Pergamon Press, Oxford, 1980).
17. L. Vaidman, Phys. Rev. A **49**, 1473 (1994).
18. S. L. Braunstein and H. J. Kimble, Phys. Rev. Lett. **80**, 869 (1998).
19. Esslinger *et al*, Phys. Rev. Lett. **94**, 210401 (2005); Ito *et al.*, Phys. Rev. Lett. **76**, 4500 (1996).